Proceedings of ISINN-30, JINR, E3-2024-42, Dubna, 2024, p.92 – 107

Effect of Nanoclay Filler on the XLPE Thermal and Shielding Properties

Elsayeda F. Salem[1], Walaa Abd-Elmonem El-Kattan[2], Nesreen R. Abdelwahab[2]

[1]*Nuclear Law and Nuclear Licenses Department, Nuclear and Radiological Safety Research Center, Egyptian Atomic Energy Authority, Cairo13759, Egypt*

[2]*Radiation Safety Department, Nuclear and Radiological Safety Research Center, Egyptian Atomic Energy Authority, Cairo13759, Egypt*

Polymers play an essential role in both industry and medical fields due to their diverse and adaptable properties. In this work, XLPE samples with hydrophilic bentonite nanoclay fillers ($H_2Al_2O_6Si$) at (1, 2.5, 4, and 5 wt%) concentrations were prepared to improve their flame-retardant and radiation shielding efficiency. The flame retardant and thermal stability parameters were investigated. The produced XLPE/$H_2Al_2O_6Si$ nanocomposite polymer sheets were exposed to a collimated beam of fast neutrons using an Am/Be neutron source with an activity of 5 Ci. In addition, the produced polymer sheets were exposed to gamma radiation using a ^{137} Cs point source with an activity of 5 μCi to test their radiation shielding properties. The result indicated uniform dispersion of nanoclay particles contributes to the enhanced thermal properties of the composite and creates a char layer that acts as a barrier slowing the thermal decomposition and reducing the heat release rate. The oxygen index rose from 28% to 34%, and there is an improvement in the burning rate according to an increase in the nanoclay wt% concentration. Absorption and the optical band gap calculations value decreased as the filer concentrations increased. The radiation attenuation capabilities increased by about 40% for neutron and 30% for gamma radiation compared to XLPE zero nanoclay filler. The findings concluded that nanoclay fillers were incorporated into XLPE to enhance its shielding capabilities; furthermore, its flame resistance properties are increasing. The prepared samples can be used in many industry applications.

Keywords: Cross-linking polyethylene (XLEP), Nanocomposite, Phy-X software, Flammability, Shielding material

1. Introduction

Polymer materials are widely used around the world in different industrial and medical applications. Due to their flexibility and biocompatibility, polymers are indispensable for creating innovative solutions across a wide range of applications [1]. In the medical industry, polymer materials provide increased flexibility in the packaging of diagnostic equipment. Because polymer materials are lightweight, flexible, and customizable, they are becoming more important in radiation shielding. Their capacity to form nanocomposites and composites improves their shielding qualities, which makes them appropriate for a variety of uses in the nuclear, medical, and industries.

Polyethylene and its composites provide effective protection while being more affordable and easier to handle as an alternative to conventional shielding materials like lead [2]. Cross-linked polyethylene (XLPE) polymer is resistant to various chemicals, oils, and solvents and is thus used in industrial applications. The fundamental component of XLPE is Low-density polyethylene (LDPE). XLPE is a thermosetting polymer commonly used in insulating cables and wires due to its thermal stability and excellent electrical properties [3]. The cross-linking process used in XLPE manufacturing improves its resistance to heat and

flames. The polymer chains are chemically bonded during cross-linking, creating a three-dimensional network structure [4]. This cross-linked structure helps to prevent the spread of fire and restricts the release of combustible gases. Halogen-free XLPE is used in industries where fire safety is a priority. Consequently, it has also found applications in the medical industry. Research has examined the use of XLPE in medical cables, catheters, and implantable devices. XLPE is commonly used in various industries due to its excellent electrical properties, thermal stability, biocompatibility, and chemical resistance. According to Saad Alshahri et al., the addition of Bi_2O_3 nanofiller to LDPE increased the composite density and significantly enhanced the protection efficiency of the LDPE polymer [5]. However, nanofilled XLPE may lack certain properties required for specific applications, such as effective protection. The incorporation of nanoclay fillers into XLPE has been shown to enhance its protective properties. With the increasing prevalence of nanoparticles in recent decades, particle composites have garnered significant attention in the field. To enhance the thermal properties of nanocomposites without compromising other characteristics, it is essential to use nanoparticles at low concentrations. Recent studies have reported the development of polymers utilizing nanocomposite concepts to enhance their properties and improve the service life and reliability of insulators [6–15]. Nanoclays derived from natural minerals are among the most studied and commercially used polymeric nanofillers [16]. The most widely utilized type of nanoclay is montmorillonite (MMT), also known as bentonite. MMT/bentonite features a 2:1 sheet structure and significantly influences the mechanical and thermal properties of polymers, even at low concentrations within the polymer matrix [17]. This increases the overall density of the material, which is beneficial for protecting against radiation, including neutrons. Neutrons are highly penetrating radiation, and effective shielding materials are required to protect personnel and equipment from their harmful effects. Shielding materials are critical in several areas, such as nuclear and radiological facilities, hospitals, and scientific research. Although XLPE is less commonly used for radiation protection compared to specialized materials such as lead or concrete, it can still offer some degree of radiation protection in specific applications. In these studies, hydrophilic bentonite nanoclay ($H_2Al_2O_6Si$) was used as a filler in XLPE at different concentrations (0, 1, 2.5, 4, and 5 wt%). The flame retardant, thermal stability, and shielding properties are tested.

2. Experimental and instruments

2.1. Samples preparation

Table 1. Thickness and density of XLPE samples with different concentrations.

Sample	XPL %	Nanoclay %	Thickness (mm)	Density (cm/gm^3)
R	100	0	1.5	0.923
W	99	1	1.6	0.98
X	97.5	2.5	1.7	1.2
Y	96	4	1.75	1.4
Z	95	5	1.8	1.6

Cross-linked polyethylene (XLPE), which is produced using low-density polyethylene (LDPE), was supplied by El-Sewedy Electric Egyplast. LDPE was mixed with Luperox 231M90 ($C_{16}H_{34}O_4$), which is used as a cross-linking agent in the polymerization of LDPE, blended with the IRGANOX B 225 component ($C_{42}H_{63}O_3P$), which is a phosphite antioxidant,

and added to IRGANOX PS 802 with the chemical formula ($C_{73}H_{108}O_{12}$). XLPE was blended with nanoclay hydrophilic bentonite ($H_2Al_2O_6Si$), purchased from Aldrich Chemistry. Table 1 shows the sample density, thickness, and concentration. Table 2 displays the fraction weight of the elemental composition.

Table 2. Elemental composition in mass fractions (wt%).

Element	R	W	X	Y	Z
H	9.434	9.35077	9.225925	9.10108	9.01785
C	90.566	89.66034	88.30185	86.94336	86.0377
O	0	0.53333	1.333325	2.13332	2.66665
Al	0	0.3	0.75	1.2	1.5
Si	0	0.15556	0.3889	0.62224	0.7778
Total	100	100	100	100	100

2.2. Samples morphology and physical characterization

Nanocomposite sample morphology and characterization were investigated using SEM and FITR. SEM (Scanning Electron Microscope) S50 with low vacuum and a resolution of 3 nm scanning at 30 kV was used. FTIR (Fourier Transform Infrared Spectroscopy), a Bruker spectrometry, was used to analyze samples in the wavelength range of 4000–400 cm^{-1}.

2.3. Thermal Analysis

The TG-50 instrument from Shimadzu (Japan), which performs thermogravimetric analysis (TGA) at a 10°C heating rate per minute, was used to investigate thermal stability for XLEP/nanoclay samples.

2.4. Flame retardant tests

Flame propagation behavior measurements for the prepared XLPE/nanoclay samples were carried out using a UL-94 flame chamber in accordance with ASTM D635-18 [16]. Sample sheets had dimensions (10 cm length, 3 cm width, and 1.5 mm thickness). LOI and burning tests are carried out at room temperature, according to the standard test method ISO 4589.

2.5. Shielding properties measurements

2.5.1. Gamma-rays

The gamma rays utilized in the measurements were a collimated beam of ^{137}Cs (5μCi) with an energy of 0.662 MeV. A multichannel analyzer with 16 K channels and a NaI (TI) scintillation detector (Oxford model) with amplifier were used to measure the gamma exposures. Fig. 1 shows the geometrical configuration of the gamma ray measurement experiment.

The radiation transmission can determine (μ_m), the coefficient of mass attenuation for the various samples at different energies. According to Beer-Lambert's law, a gamma-ray beam with intensity I_0 will attenuate as it passes through a thickness X of the material, as in Equation 1 [17]:

$$I(x) = I_0 e^{-\mu x} , \quad (1)$$

μ represents the linear attenuation coefficient. For a sample with density ρ, the total mass attenuation coefficient (μ_m) is expressed as follows:

$$\mu_m = \frac{\mu}{\rho}, \tag{2}$$

μ_m has been calculated for the investigated samples using Phy-X program [18].

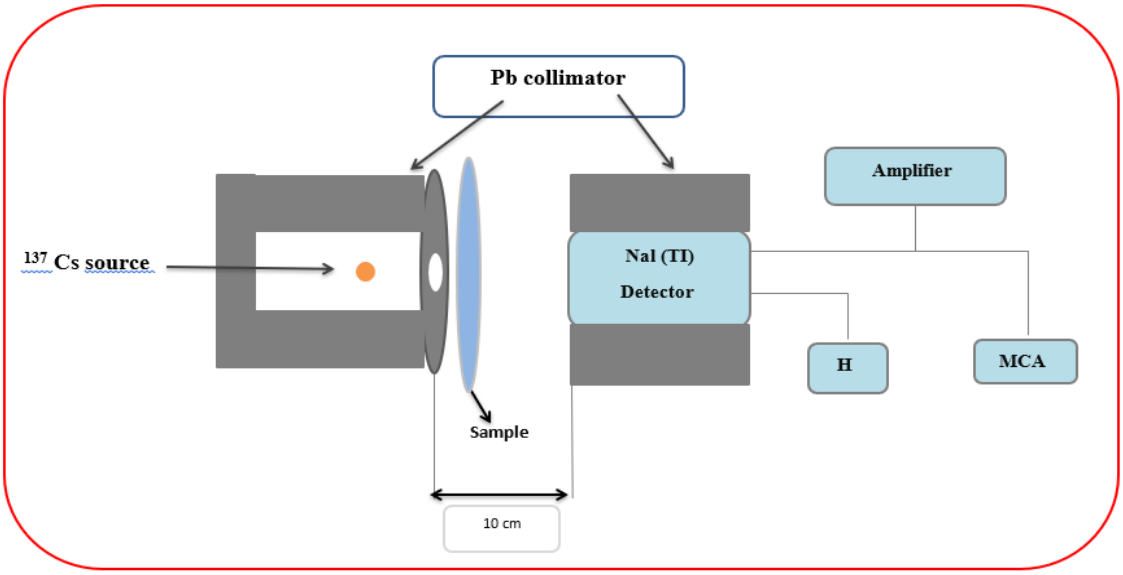

Fig. 1. Experimental setup of gamma shielding measurements.

HVL (cm) is the half-value layer, TVL (cm) is the tenth-value layer, and the mean free path of the photon (λ) are illustrated as follows:

$$\text{HVL} = \frac{ln2}{\mu} \quad \& \quad \text{TVL} = \frac{ln10}{\mu} \quad \& \quad \lambda = \frac{1}{\mu}. \tag{3}$$

2.5.2. Neutron attenuation

The measurements for the experiment were obtained using a collimated beam of neutrons from a ^{241}Am-Be neutron source with activity (5 Ci), which emitted a mean energy of approximately 4.25 MeV. The monitor detector detected the neutron dose rate before and after using the shielding sample. Fig. 2 shows the geometrical arrangement.

The monoenergetic neutron parallel beam is attenuated as it travels through a material due to absorption and dispersion. The removal cross-section (Σ_R) concept is based on the presence of hydrogen in the shielding material. The formula $\Sigma_R = \Sigma t$, where Σt represents the total macroscopic cross-section, can be used to calculate the attenuation of fast neutrons through a hydrogen-containing material. This assumes that a collision with hydrogen is comparable to an absorption event [18]. Σ_R for homogeneous mixtures and compounds can be calculated as follows:

$$\Sigma_R = \sum \rho_i (\Sigma_R/\rho)_i \ \ (\text{cm}^{-1}), \tag{4}$$

where ρ_i is the partial density. The mean free path λ was calculated using the formula $\lambda = 1/\Sigma_R$ [19].

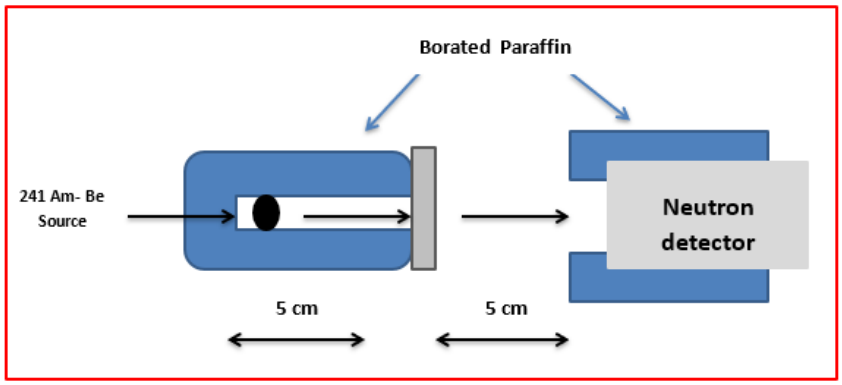

Fig. 2. Schematic diagram of neutron shielding measurement setup.

3. Results and discussion

With FTIR, one can see the chemical structure of a reaction and gain insight into how reactant molecules bind and interact to generate the final product. Fig. 3 shows the XLPE/$H_2Al_2O_6Si$ nanocomposite sheet's FT-IR spectrum compared to pure XLPE. The peaks of pure XLPE at 2914 and 2848 cm^{-1} are due to the stretching of the -CH2 groups, both symmetric and antisymmetric in polyethylene. Peaks falling between 1472 and 1460 cm^{-1} are attributed to the -CH_2 and -CH_3 groups deforming. Long chains of CH_2 in XLPE are characterized by peaks at 720–730 cm^{-1} [20–22]. A few hydrogen-bonded hydroxyl groups, as indicated by the weak bands at 3210–3590 cm^{-1}, disappeared after nanoclay was added. Also, sharpness and stretching in the peaks were noticed. The 945 and 950 cm^{-1} peaks are attributed to Si-OH and Al-OH, respectively [23, 24]. It is evident from the incorporation of nanoclay into the XLPE matrix. Fig. 4 shows the microstructure SEM images of pure XLPE and XLPE/nanoclay samples with (0.5, 1, 2.5, and 5 wt%) concentrations. It is obvious that it is uniformly distributed and lacks protrusions. Nanoclay fillers, because of their tiny size and large surface area, are often dispersed evenly within the XLPE matrix.

Thermogravimetric Analysis (TGA): TGA has determined the prepared samples' thermal degradation at elevated temperatures. The weight of the sample is determined in dependence on temperature. Fig.5 (a & b) shows the TGA and derivative TGA curves (DTGA) for prepared XLPE/$H_2Al_2O_6Si$ Clay nanocomposite samples**.** Because of the volatile substance in the composition, there is an initial weight loss between 280 and 460 °C. The total weight loss of XLPE/nanoclay is lower than that of pure XLPE. We notice that nanoparticles contribute to the rise of thermal degradation temperature, where sample Z has achieved the highest thermal stability with a 5 wt% nanoclay concentration. This is so that additional breakdown of the underlying polymer is stopped by the layer of nanoparticles that forms on the polymer's surface and acts as a barrier [25]. Fig. 5(b) clearly shows the principal weight loss temperature increasing from 478 °C for pure XLPE to 489°C with adding nanoclay 5% wt, showing good thermal stability for sample (Z). It also demonstrates the sample's thermal resilience and the fact that XLPE chains break down at relatively low temperatures. The thermal stability of the XLPE matrix was enhanced by the nanoclay filler being added.

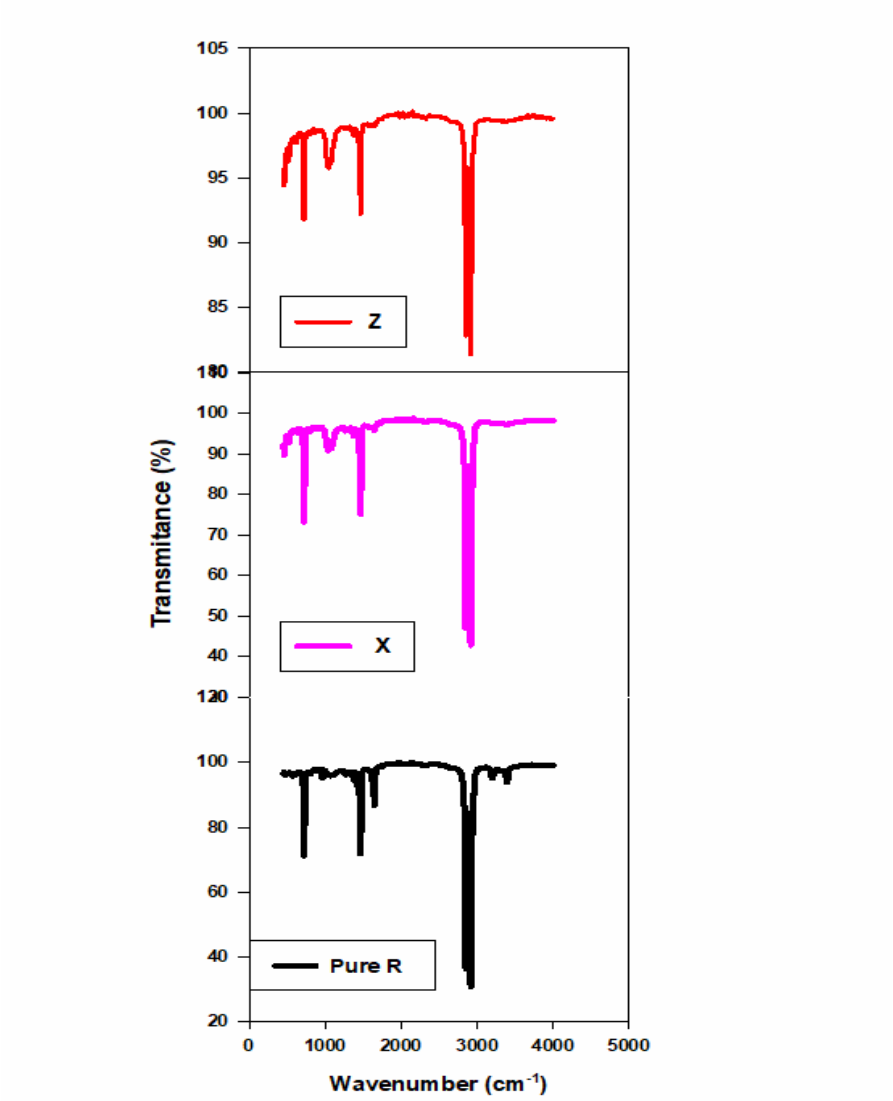

Fig. 3. FTIR spectra of pure XLPE and XLPE/Clay nanocomposite sample.

Ignition test: Burning UL-94H test and burning spread rate for pure XLPE and XLPE/Clay nanocomposite samples with different concentrations are shown in Fig. 6 and Fig.7 (a & b), respectively. It is evident that the LOI of the blank sample was about 28, and adding nanoclay to XLPE samples improved its value to 34. From Fig. 6-b, it is noticed that the LOI of XLPE value was directly proportional to nanoclay additives concentration, where sample Z, which has a 5% weight concentration of nanoclay, has the highest value. As seen in Fig. 7-a, pure XLPE burns at a rate of 18.7 mm/min. Nevertheless, the burning rate dropped to 9.6 mm/min after adding 2.5% wt.

Similarly, the burning rate for the sample containing 5% wt of nanoclay dropped to 4.4 mm/min. During combustion, droplets formed despite the pure XLPE sample having a short flame spread rate. Samples Y and Z achieved the UL-94H-0 grade without leaking, as shown in Fig. 6. According to the results, sample Z had a 27% increase in LOI value and a 65% decrease in burning rate compared to sample R. The $H_2Al_2O_6Si$ nanoparticles accumulate on the surface of the burning polymer, creating a barrier that acts as physical protection from heat

and slowing down the volatilization of the pyrolysis-generated polymer fragments. This barrier of the char layer acts to oxygen diffusion and heat transfer, effectively suppressing flame propagation and reducing the burning rate.

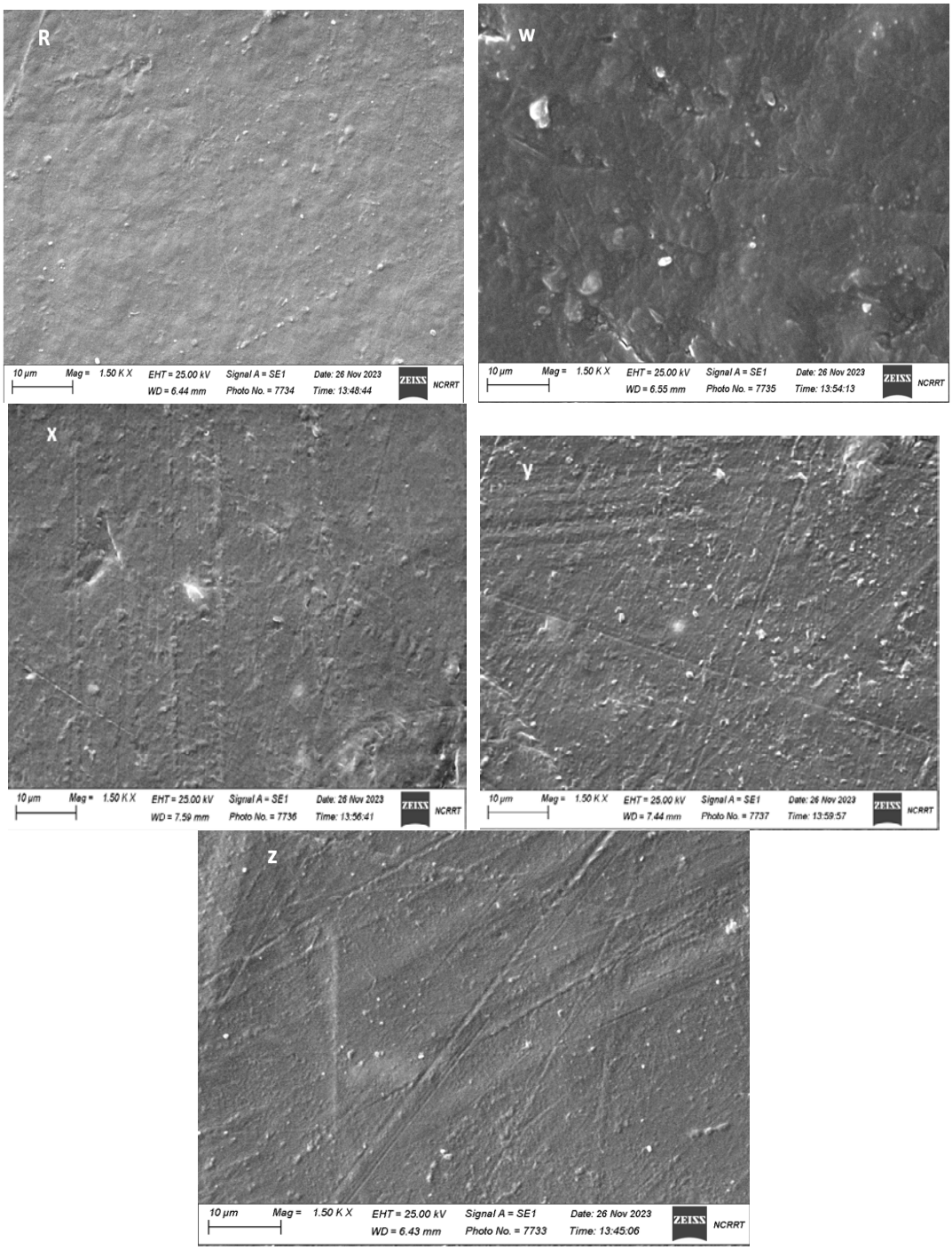

Fig. 4. SEM of samples of pure XLPE and XLPE/Clay nanocomposite of different concentrations.

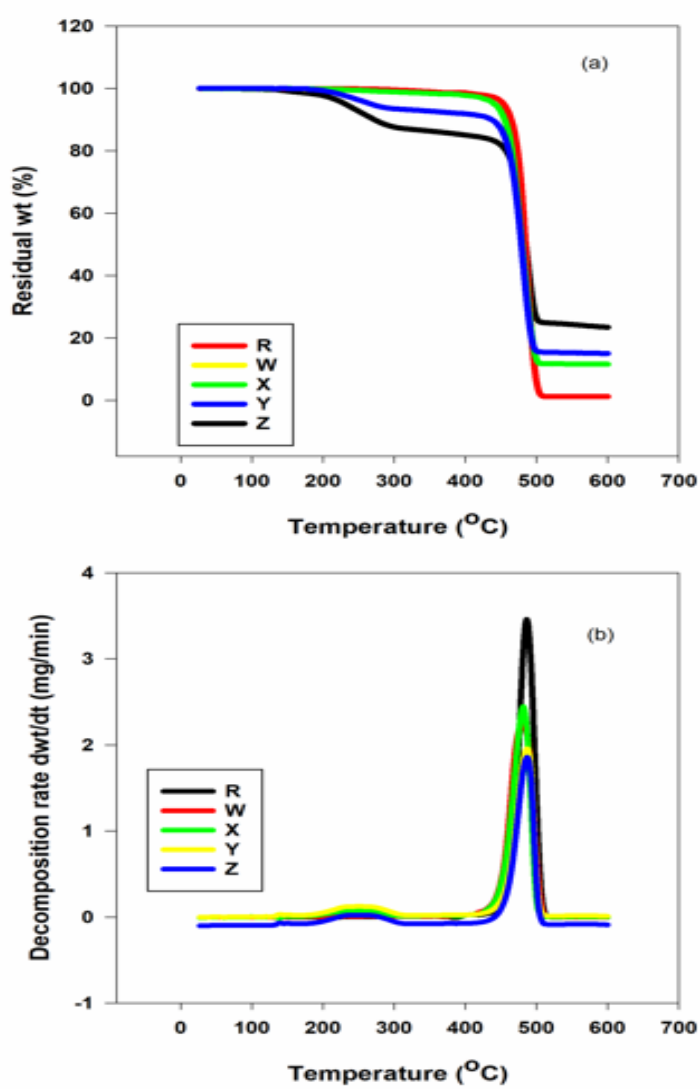

Fig. 5. TGA and DTG curves of pure XLPE and XLPE/Clay nanocomposite sample.

Optical properties: Absorption spectra as a function of UV wavelength (λ) for XLPE and XLPE/nanoclay with different concentration samples are shown in Fig. 8. The absorbance ratings increase upon increasing nanoclay wt.% concentration, which indicates the positive effect of nanoclay filer amount on absorption properties of XLPE. Furthermore, absorbance has the highest values for λ range (200−300) nm, and then a rapid decrease occurs for λ = 320 to 400. For λ > 400 nm, absorption is not affected by increasing wavelength and remains almost constant. The absorption maximum from 200−300 nm originates from the electronic oscillation of conjugated double bonds –$(CH=CH)_2$– and –$(CH=CH)_3$ [26]. If the wavelength is more significant than 300 nm, at 450 nm, the absorbance decreases gradually. For λ> 450 nm, the increase of λ does not affect absorbance. Adding nanoclay, hydrophilic bentonite ($H_2Al_2O_6Si$) nanoclay filler to an XLPE could improve UV absorption, thereby reducing the damage to its bonds and augmenting the ion of the XLPE system [27]. Utilizing the layered structure of nanoclays, particularly montmorillonite-type clays, can create a tortuous path for UV radiation within the XLPE matrix. This leads to increased absorption through multiple scattering events and interlayer interactions. The Beer-Lambert law states that the absorbance

coefficient α measures how much light or electromagnetic radiation a material absorbs per unit distance traveled. It is in units of inverse length $(cm)^{-1}$.

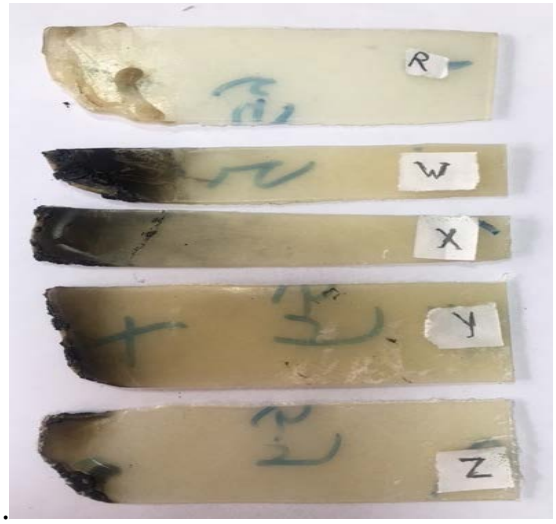

Fig. 6. Burning test for pure XLPE and XLPE/Clay nanocomposite samples of different concentration.

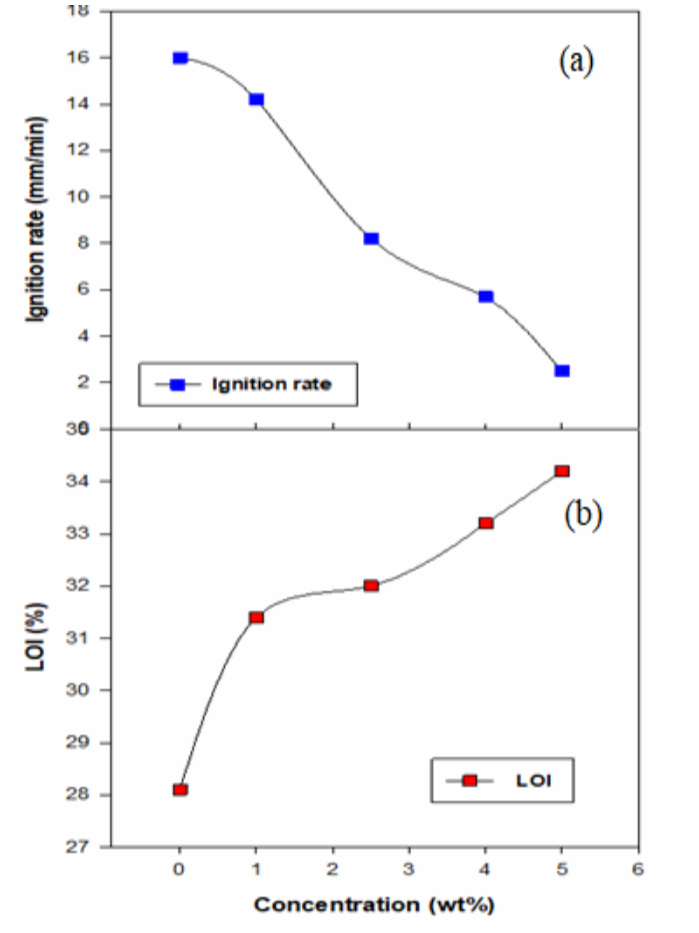

Fig. 7. Flame spread rate of burning (a) LOI (b) for pure XLPE and XLPE/Clay nanocomposite with concentrations.

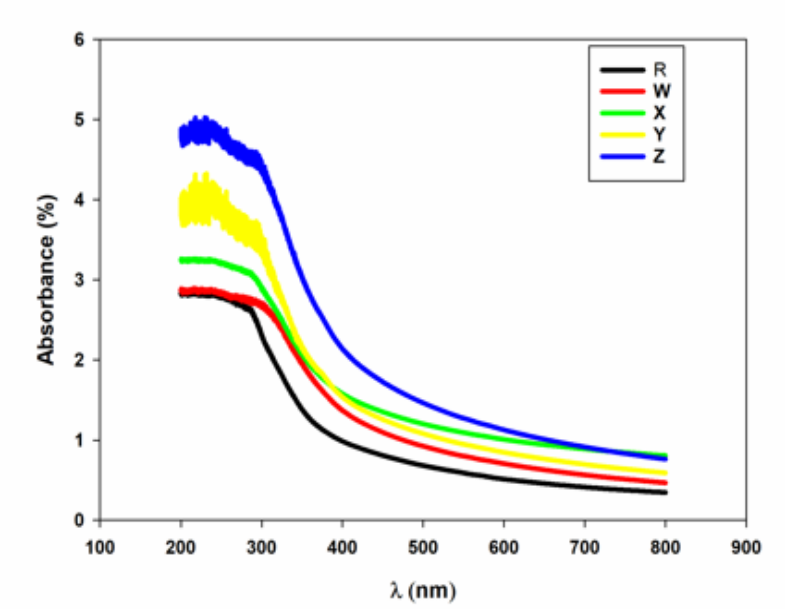

Fig. 8. Absorbance spectrum of pure XLPE and XLPE/Clay nanocomposite sample versus wavelength.

The optical band gap of a material represents the minimum energy for an electron transition, thus allowing the material to absorb photons of specific energies.

Then the optical band gap (E_g) of XLPE can be measured as: $(\alpha E)^{1/n} = X(E - E_g)$, where E is the photon energy [28]. The $1/n$ value is related to direct and indirect transitions 0.5 and 2, respectively. Fig.9 shows the $(\alpha E)^{0.5}$ versus photon energy (E) for the investigated samples. It appears that XLPE has an optical band gap (E_g) of 2.7 eV, smaller than the optical band gaps of high-density polyethylene and low-density polyethylene, which have optical band gaps of 5.44 eV and 7.4 eV, respectively, before any treatments or aging processes [29]. XLPE, the cross-linking process likely affects its optical properties, resulting in a smaller band gap than other polyethylene forms. The indirect band gap decreases as nanoclay wt% content increases. The structure resonance develops in the density of states, consequently splitting off the bands due to the increasing concentration of nanoclay. A smaller optical band gap implies that the material can absorb lower energy photons, corresponding to longer wavelengths. As a result, the absorption spectrum of the material shifts towards longer wavelengths. notice that the optical band gap is an important parameter as it provides insights into the optical properties of the material, which in turn influences its performance in various applications. Adding nanoclay to XLPE can affect its optical properties, depending on the concentration of nanoclay used and its dispersion within the polymer matrix.

3.1. Gamma shielding results

Fig. 10 illustrated μ through the XLPE samples as a function of nanoclay wt % filler, measured using point source ^{137}Cs with energy 0.662 MeV. Table 3 represents μ, μ/ρ, HVT, and λ for XLPE/nanoclay samples. It is noticed that μ increases as the wt % of nanoclay increases because of the high atomic number of elements in nanoclay hydrophilic bentonite ($H_2Al_2O_6Si$). This can result in numerous interactions between photons and material particles, which can cause photon energy to be lost and then improve the scattering of gamma rays, thereby enhancing the XLPE shielding properties. The material's capability to attenuate gamma rays increases with increasing the probability of interaction with matter [30]. When

the $H_2Al_2O_6Si$ nanoclay content increases, the mass attenuation coefficient value μ/ρ decreases due to increased sample density. Adding 5wt% $H_2Al_2O_6Si$ nanoclay to XLPE polymer improves gamma attenuation by about 54%. We use Win XCOM software to simulate the mass attenuation coefficient, and μ values of XLPE and XLPE/ nanoclay samples are shown in Table 3. It can be known that the values of the five samples are all less than 5%. The experimental values of μ/ρ agreed with that of theoretical values obtained from WinXCom.

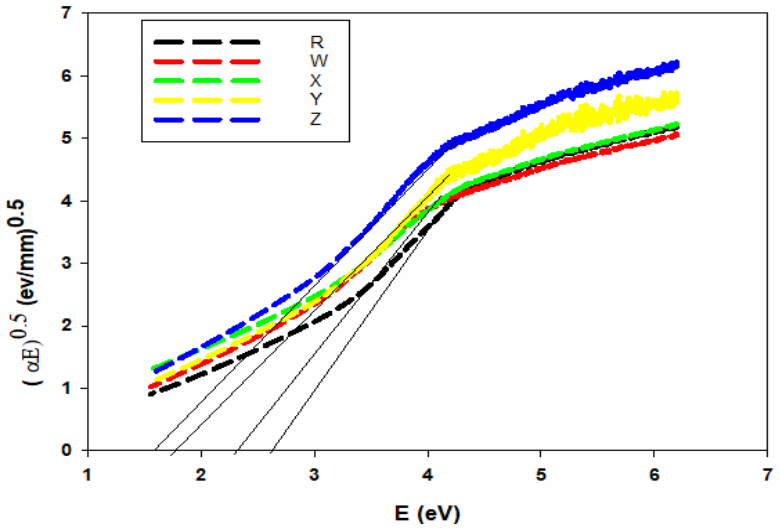

Fig. 9. Optical band gap for pure XLPE and XLPE/clay nanocomposite samples of varying concentrations.

Table 3. μ, μm, HVL and λ for shielding composites using 137Cs (662 keV).

Sample	μ (cm^{-1})		μ_m (cm^2/g)		HVL (cm)		λ (cm)	
	Measured	Calculated	Measured	Calculated	Measured	Calculated	Measured	Calculated
R	0.077 (4)	0.077 (4)	0.084	0.0843	8.973	8.904	12.945	12.848
W	0.082 (4)	0.082 (4)	0.084	0.0842	8.423	8.393	12.152	12.111
X	0.100	0.101	0.083	0.08415	6.924	6.863	9.989	9.903
Y	0.117	0.118	0.082	0.0840	5.945	5.900	8.577	8.499
Z	0.133	0.134	0.081	0.0844	5.215	5.158	7.523	7.443

Sample Z has lower HVL and λ as shown in Fig.10. Under the same thickness, materials with lower HVL and λ values will provide enhanced radiation shielding [31].

Neutron shielding properties of XLPE: Equation 4 was used to determine Σ_R and the mean free path (λ) for XLPE with different concentrations of H2Al2O6Si nanoclay. The results are shown in Fig. 12(a) and Fig. 12(b). Σ_R values increase with increasing nanoclay filler concentrations. However, the sample (Z) has approximately double the value of the XLPE pure sample (R) at 5wt%, Σ_R rise. It is evident that Σ_R values depend on the type and density of the components that compose shields [32]. The neutron parameters (Σ_R and λ) of the studied samples are shown in Table 4, together with their theoretical and experimental values. The calculated and measured values agree closely. Samples are shown in Table 4, together with

their theoretical and experimental values. The calculated and measured values agree closely, and λ decreases as the ($H_2Al_2O_6Si$) nanoclay increases. For sample (Z), λ decreases by about 40%. Fig.12(a & b) shows that the investigated sample is more effective for neutron shielding than gamma radiation. The concentration and distribution of nanoclay fillers, the material's thickness, and thermal stability all affect how successful nanoclay enhanced XLPE is at shielding neutrons.

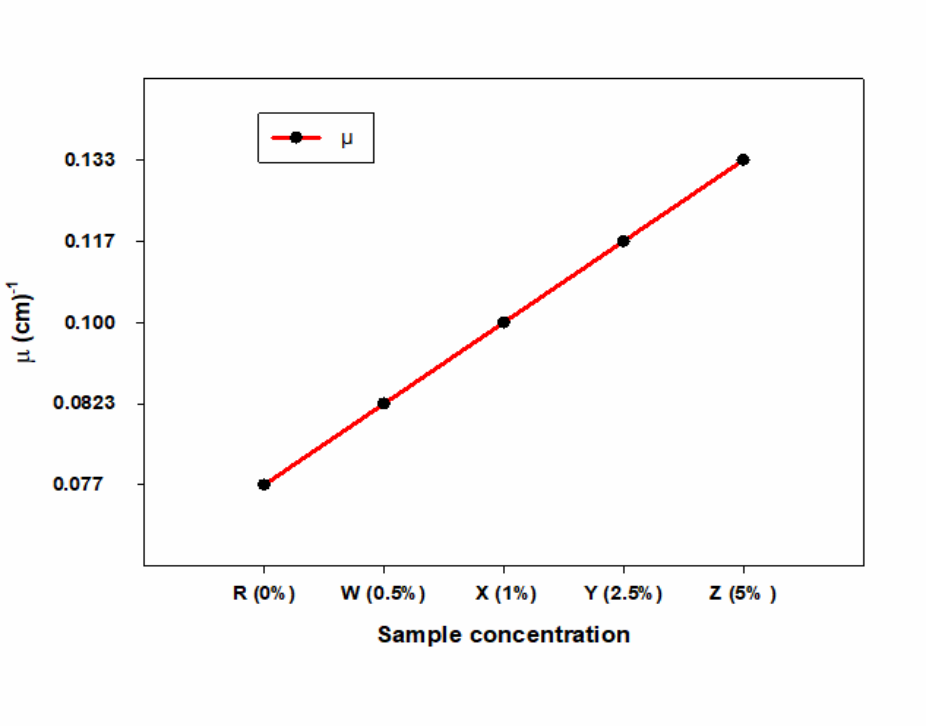

Fig. 10. Linear attenuation coefficient of gamma radiation for XLPE/nanoclay at various concentrations.

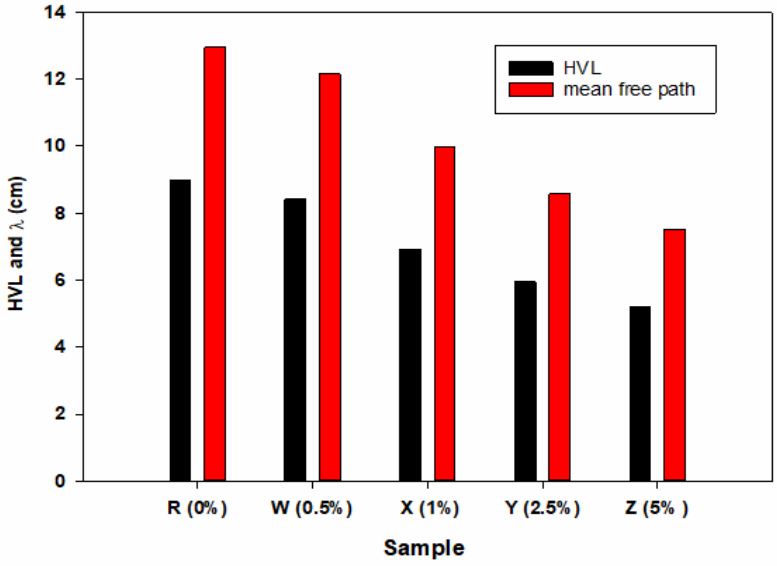

Fig. 11. HVL and λ for XLPE samples prepared with different nanoclay wt% concentrations.

Table 4. Σ_R and λ for XLPE samples with different nanoclay concentrations.

Sample	Σ_R (cm^{-1})		λ (cm)	
	Experiment	N-Xcom	Experiment	N-Xcom
R	0.189	0.188	5.291	5.317
W	0.191	0.188	5.236	5.320
X	0.241	0.240	4.149	4.174
Y	0.279	0.276	3.584	3.224
Z	0.319	0.313	3.135	3.196

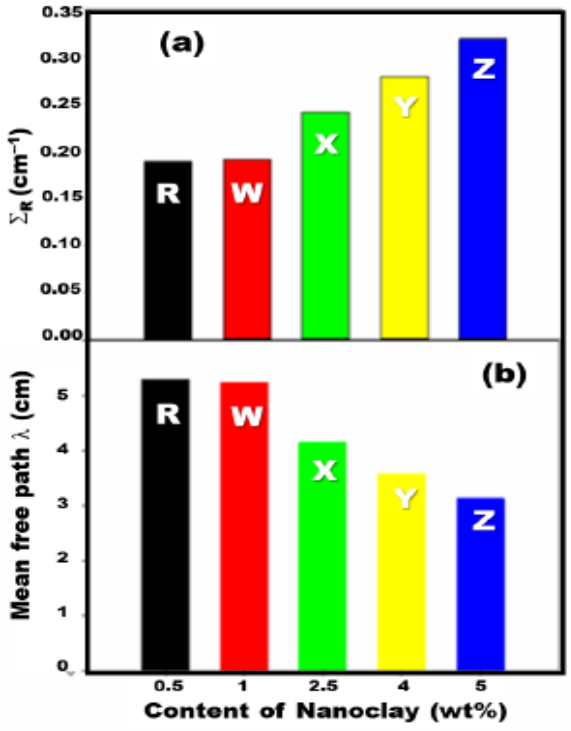

Fig. 12. (a) − Removal cross-section coefficient (Σ_R), (b) − mean free path (λ) of a fast neutron for XLPE with different nanoclay wt% concentrations.

4. Conclusion

The study focused on improvement to the XLPE/nanoclay composite in fire resistance and radiation protection. Incorporating XLPE with nanoclay fillers enhances thermal stability by acting as a thermal barrier. The high surface area and layered structure of nanoclays create tortuous diffusion paths for heat transfer, thereby retarding thermal degradation processes in the polymer matrix. With their layered structure, the physical barrier created by $H_2Al_2O_6Si$ nanoclay fillers hinders the diffusion of flammable gases and heat transfer during combustion. This barrier effect can slow the spread of flames and reduce the intensity of the fire. The presence of nanoclays helps mitigate UV radiation's effects on the polymer matrix, leading to reduced degradation rates and improved long-term performance, particularly in outdoor or UV-exposed applications. Nanoclay fillers can increase the overall UV absorption capacity of XLPE nanocomposites. Nanoclays may possess intrinsic UV-absorbing properties or act as UV attenuators by providing additional surface area for UV absorption, resulting in a broader spectrum and higher UV absorption efficiency than pure XLPE. A material's molecular structure, level of cross-linking, crystallinity, and presence of any additives or impurities can

all affect its optical band gap. Nanoclay hydrophilic bentonite ($H_2Al_2O_6Si$) filler improved absorption and scattering of UV and gamma rays, thereby enhancing XLPE shielding effectiveness. Nanoclay particles have high aspect ratios and large surface areas, which allow them to effectively interact with radiation and improve the material's shielding properties. Nanoclay fillers can be incorporated into XLPE to enhance its neutron shielding capabilities. By dispersing nanoclay fillers within the XLPE matrix, the ability of the material to attenuate neutrons can be significantly improved. ($H_2Al_2O_6Si$) nanoclay fillers offer the potential for enhancing the neutron shielding properties of XLPE and could contribute to the development of more efficient and lightweight shielding materials for various applications.

Acknowledgments: I would like to extend my heartfelt gratitude to my advisor Professor Gamal Sadek Professor of Experimental Nuclear Physics at Al-Azhar University for his support throughout this study.

References

1. Brydson, J.A. "Plastics Materials," 7th Edition, Butterworth-Heinemann, 1999.
2. S.M.J. Mortazavi, M. Kardan, S. Sina, H. Baharvand, N. Sharafi, Design and fabrication of high density borated polyethylene nanocomposites as a neutron shield. volume 14, No 4 International Journal of Radiation Research, October 2016.
3. Abdelrahman Said, M.A. Abd-Allah , Amira G. Nawar , Alaa E. Elsayed , and Samir Kamel, Enhancing the electrical and physical nature of high voltage XLPE cable dielectric using different. J Mater Sci: Mater Electron (2022) 33:7435–7443.
4. A. Thabet, Effect of nanoparticles on water treeing characteristics in XLPE industrial insulating materials. J. Eng. Sci 40 (2012) 208–191.
5. Saad Alshahri, Mohammed Alsuhybani, Eid Alosime , Mansour Almurayshid, Alhanouf Alrwais and Salha Alotaibi, LDPE/Bismuth Oxide Nanocomposite Preparation Characterization and Application in X-ray Shielding. Polymers 2021, 13, 3081. https://doi.org/10.3390/polym13183081.
6. N.M.K. Abdel-Gawad et al., Enhancement of dielectric and mechanical properties of polyvinyl chloride nanocomposites using functionalized TiO2 nanoparticles. IEEE Trans. Dielectr. Electr. Insul. 24(6), 3490–3499(2017).
7. N.M.K. Abdel-Gawad et al., Development of industrial scale PVC nanocomposites with comprehensive enhancement in dielectric properties. IET Sci. Meas. Technol. 13(1), 90–96 (2019).
8. Q. Yu et al., Properties of water tree growing in XLPE and composites, in Proceedings of the 2nd international conference on electrical materials and power equipment (ICEMPE). (IEEE, Piscataway, 2019), pp. 409–412.
9. S.H. Salh, D.A. Raswl, Thermal stability of polymer composite films based on polyvinyl alcohol doped with different fillers. J. Phys. 2, 5–10(2018).
10. A.H. Awad et al., A study of some thermal and mechanical properties of HDPE blend with marble and granite dust. Ain Shams Eng. J. 10(2), 353–358(2019).
11. M. Gi_zyn´ski, B. Romelczyk-Baishya, Investigation of carbon fiber–reinforced thermoplastic polymers using thermogravimetric analysis. J. Thermoplast. Compos. Mater. 34,(1) 126–140 (2021).
12. Ch. Zhang et al., Improved direct current electrical properties of crosslinked polyethylene modified with the polar group compound. Polymers 11(10), 1624(2019)

13. S.H. Liu et al., Improving thermal stability of polyurethane through the addition of hyperbranched polysiloxane. Polymers 11(2019) 697 ,(4)
14. Zh. Liu et al., High thermal conductivity of flake graphite reinforced polyethylene composites fabricated by the powder mixing method and the melt-extruding process. Polymers 10(2018) 693 ,(7)
15. X. Chi et al., Characterization of polypropylene modified by blending elastomer and nano-silica. Materials 11(8), 1321 (2018)
16. M. Rallini, J.M. Kenny, Nanofillers in Polymers. In Modification of Polymer Properties, Elsevier, New York, NY 2017. https://doi.org/10.1016/B978-0-323-44353-1.00003-8.
17. M. Çelı, M. Önal, O. Erref,. Preparation and Characterization of Intercalated Polymethacrylamide/Na-Montmorillonite Nanocomposites. Chem. Mater. Res. 2017;1325. doi:10.1080/10601320600653806.
18. Erdem Şakar, Özgür Fırat Özpolat, Bünyamin Alım, M.I. Sayyed, Murat Kurudirek. Phy-X/PSD: Development of a user friendly online software for calculation of parameters relevant to radiation shielding and dosimetry // Radiation Physics and Chemistry. 2020. V. 166. P. 108496, https://doi.org/10.1016/j.radphyschem.2019.108496. https://phy-x.net/module/physics/shielding/.
19. ISO, 1989. Road Vehicles, and Tractors and Machinery for Agriculture and Forestry—Determination of Burning Behaviour of Interior Materials. International Organization for Standardization, Switzerland.
20. Garber, D.I., Kinsey, R., 1976. Neutron cross sections; v 2, curves. Brookhaven Nat. Lab. Ghobashy, M.M., Khozemey, E., 2018. Sulfonated gamma-irradiated blend poly (styrene/ethylene-vinyl acetate) membrane and their electrical properties. Adv. Polym.Technol. 37, 1249–1255
21. Blizard, E., Abbott, L., 1962.Shielding. In: Reactor Handbook, vol. III Part B. Inter 12 Science Publishers, New York.
22. A.M. El-Khayatt., NXcom – A program for calculating attenuation coefficients of fast neutrons and gamma-rays., Annals of Nuclear Energy Journal, Volume 38, Issue 1, January 2011, Pages 128-132
23. Gaston, F.; Dupuy, N.; Marque, S.R.; Barbaroux, M.; Dorey, S. One year monitoring by FTIR of -irradiated multilayer film PE/EVOH/PE. Radiat. Phys. Chem. 2016, 125, 115–121.
24. Socrates, G. Infrared and Raman Characteristic Group Frequencies, 3rd ed.; John Wiley & Sons: Hoboken, NJ, USA, 2001.
25. Xu, A.; Roland, S.; Colin, X. Physico-chemical characterization of the blooming of Irganox 1076® antioxidant onto the surface of a silane-crosslinked polyethylene. Polym. Degrad. Stab. 2020, 171, 109046. [CrossRef]
26. Liang, Y., Ouyang, J., Wang, H., Wang, W., Chui, P., Sun, K. Synthesis and characterization of core–shell structured SiO2@ YVO4: Yb3+, Er3+ microspheres. Appl. Surf. Sci. 2012, 258, 3689–3694.
27. Li Cui, Holly J. Butler, Pierre L. Martin-Hirsch and Francis L. Martin, Aluminium foil as a potential substrate for ATR-FTIR, transflection FTIR or Raman spectrochemical analysis of biological specimens. Journal, The Royal Society of Chemistry 2016.
28. M.F. Ashby a, Y.J.M. Bréchet , Designing hybrid materials. Acta Materialia, Volume 51, Issue 19, 25 November 2003, Pages 5801−5821.
29. Y. Zhang, Z. Hou, K. Wu, S. Wang, J. Li, and S. Li, “Influence of oxygen diffusion on thermal ageing of cross-linked polyethylene cable insulation.,” Materials (Basel, Switzerland), vol. 13, 2020.

30. Chris Rockett, "UV Degradation Effects in Materials – An Elementary verview".UV solution, innovation for industry , public health and the environment, 12- 2019.
31. H.G. Harish Kumar, R.D. Mathad, S. Ganesh, K.S.S. Sarma, and C.R. Haramaghatti, “Electron beam induced modifications in high density polyethylene,” Braz. J. Phys., vol. 41, pp. 7-14, 2011.
32. Shiyu Yin, Hao Wang , Shifeng Wang, , Jing Zhang and Yuanzhi Zhu, “Effect of B2O3 on the Radiation Shielding Performance of Telluride Lead Glass System” Crystals 2022, 12, 178.
33. Issa, S.; Sayyed, M.; Kurudirek, M. “Investigation of Gamma Radiation Shielding Properties of Some Zinc Tellurite Glasses”. J. Phys. Sci. 2016, 27, 97–119. [Google Scholar] [CrossRef].
34. Elsayeda F. Salem, Ehab E. Khozemy, Amr El-Hag Ali. “Potential flame retardancy of high-density polyethylene (HDPE) composite for possible use as a radiation shield”. Journal, Progress in Nuclear Energy, 165 (2023) 104900.